Two-photon spectroscopy of ZnSe under uniaxial stress

D. Fröhlich and W. Nieswand
Institut für Physik, Universität Dortmund, D-44221 Dortmund, Germany

U. W. Pohl
Institut für Festkörperphysik, Technische Universität Berlin, D-10623 Berlin, Germany

J. Wrzesinski
Institut für Physik, Universität Dortmund, D-44221 Dortmund, Germany
(Received 30 May 1995; revised manuscript received 2 August 1995)

Resonances on the upper transverse polariton branch of ZnSe are studied under uniaxial stress by two-photon excitation spectroscopy. Due to the small linewidth, shifts and splittings are clearly resolved and the hydrostatic, tetragonal, and trigonal deformation potentials are determined with high accuracy.

I. INTRODUCTION

II-VI semiconductors and among them especially ZnSe have recently gained increasing interest because they are good candidates for blue-emitting laser diodes. In the first ZnSe-based laser diode a ZnSe waveguide with a ternary $Cd_xZn_{1-x}Se$ single quantum well was used for the device emitting in the blue-green spectral range at 77 K.[1] Later, considerable improvement towards higher temperature, shorter wavelength, and even cw operation was achieved by use of quaternary layers on GaAs substrates.[2–6] Most of the layers are considerably stressed due to lattice mismatch and different thermal expansion coefficients. The stress-induced shifts and splittings of the electronic transitions are described by the deformation potentials. The determination of these fundamental parameters is therefore of great relevance for further practical developments. As recently shown[7,8] for KI and CuCl, nonlinear optical methods like two- and three-photon absorption are far superior to the classical linear optical methods in experiments under uniaxial stress. Due to the usually much smaller linewidths of nonlinear resonances as compared to linear optical absorption, photoluminescence or reflection lines (Fig. 1), one can directly deduce the stress-induced splittings and shifts from the experimental data.

Furthermore, one can neglect stress inhomogeneities near the surface because the crystal is transparent for a single photon which takes part in the nonlinear process. Reflection and photoluminescence measurements, however, depend very much on the surface quality. For one-photon absorption measurements near the reststrahlen region one needs thin samples which are often already stressed due to preparation and thus not well suited for detailed measurements.

The paper is organized as follows. After a short description of the experimental setup, we present an outline of the theory for the analysis of our data. Finally, experimental results are presented and discussed.

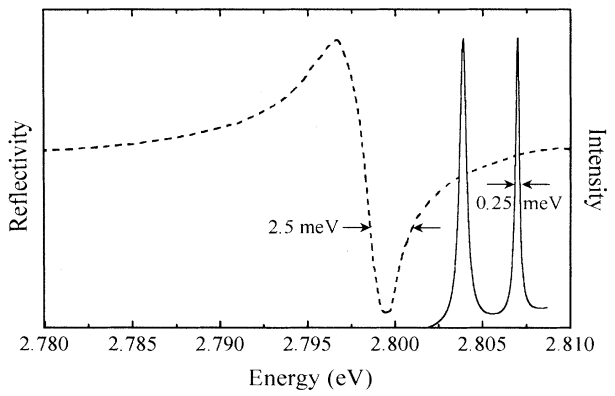

FIG. 1. Two-photon excitation spectrum of resonances on the upper polariton branch in ZnSe at 5 K (solid line). For comparison of linewidth, the reflectivity spectrum of ZnSe at 2 K from Ref. 9 is shown (dotted line).

II. EXPERIMENT

Two-photon excitation measurements are performed with a tunable dye laser (Laser Analytical Systems LDL 205) pumped by a Nd:YAG laser (Quanta Ray GCR 3a) with a repetition rate of 10 Hz. The dye laser has a pulse length of 5 ns and a typical peak energy of 8 mJ. The spectral resolution is better than 5 μeV. The laser beam is focused on the sample which is mounted in the uniaxial stress apparatus in a helium cryostat at a temperature of about 5 K. The excitation is detected by monitoring near-band-gap luminescence. A double-prism monochromator (Zeiss MM3) is used to suppress scattered light from the dye laser. The electronic signals of the signal photomultiplier and the reference diode are measured by gated integrators, digitized by analog-to-digital converters, and recorded by a computer, which also controls the wavelength setting and the polarization of the dye laser. The polarization direction of the dye laser beam is ad-

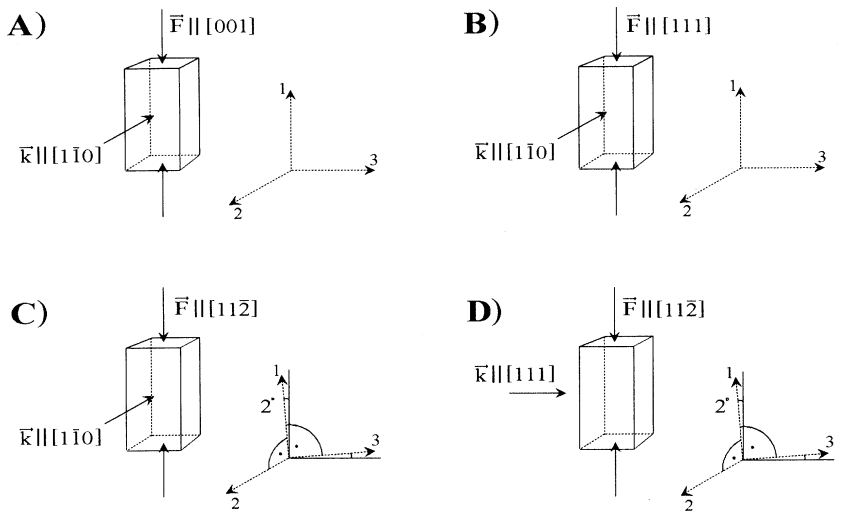

FIG. 2. Schematic diagram of the four experimental configurations **A**–**D**. The broken lines represent the orientation of the principal axes. $\vec{F}$ and $\vec{k}$ are the applied force and the total k vector, respectively.

justable parallel or perpendicular to the stress axis by a half-wave plate.

The samples are single crystals grown by seeded vapor transport in a sealed quartz ampoule using a method initially applied by Markov and co-workers.[10] Growth occurred in a hydrogen ambient at 1740 K and resulted in twin-free single crystals bounded by (110) and (111) faces. The samples are mounted on a goniometer head, oriented to better than 0.2° by x-ray Bragg reflection, directly transferred to cutting, and finally polished. The dimensions of the crystals after preparation are about $1 \times 1.5 \times 3$ mm^3.

Measurements are performed in four different configurations **A**, **B**, **C**, and **D** (Fig. 2), which are specified by the directions of the applied force $\vec{F}$ and total k vector with respect to the crystalline axes: configuration **A**, $\vec{F} \parallel [001]$ and $\vec{k} \parallel [1\bar{1}0]$; configuration **B**, $\vec{F} \parallel [111]$ and $\vec{k} \parallel [1\bar{1}0]$; configuration **C**, $\vec{F} \parallel [11\bar{2}]$ and $\vec{k} \parallel [1\bar{1}0]$; configuration **D**, $\vec{F} \parallel [11\bar{2}]$ and $\vec{k} \parallel [111]$. By proper choice of the incoming laser polarization one can selectively excite the polarization $\vec{\mu}$ of the excited state. In configurations **A** and **B** the principal axes are parallel or perpendicular to the applied stress and the total k vector. The two-photon spectra are measured for uniaxial stress up to 120 MPa.

III. THEORY

The exciton and polariton states are derived from the uppermost, fourfold-degenerate p-like valence band and the lowest, spin-degenerate s-like conduction band. The valence- and conduction-band states of zinc-blende ZnSe (point group T_d) transform according to the irreducible representations Γ_8 and Γ_6, respectively. The eightfold exciton ground state with a $1S$ envelope (Γ_1 symmetry) can be decomposed into the irreducible components (following the notation of Ref. 11):

$$\Gamma_6(2) \otimes \Gamma_8(4) \otimes \Gamma_1(1) = \Gamma_3(2) \oplus \Gamma_4(3) \oplus \Gamma_5(3). \quad (1)$$

The degeneracies of the states are given in parentheses. The Γ_3 and Γ_4 excitons are pure triplet states (paraexcitons) and are both symmetry and spin forbidden, whereas the Γ_5 states are singlet-triplet mixed states (orthoexcitons) and dipole allowed. Only the orthoexcitons can thus interact with photons and form polaritons.

The data are analyzed by use of the Hamiltonian H:

$$H = H_{\mathrm{ex}} + H_1, \quad (2)$$

$$H_{\mathrm{ex}} = \left(\frac{1}{4} - \vec{\sigma}_e \cdot \vec{\sigma_h}\right) \Delta_{\mathrm{ex}}, \quad (3)$$

$$H_1 = a\mathrm{Tr}(e) - b\left[\left(l_{h,x}^2 - \frac{l_h^2}{3}\right) e_{xx} + \mathrm{c.p.}\right] - d\left[\left(l_{h,x} l_{h,y} + l_{h,y} l_{h,x}\right) e_{xy} + \mathrm{c.p.}\right]. \quad (4)$$

H_{ex} describes the analytical part of the exchange interaction according to Cho[12] with $\vec{\sigma}_e$ and $\vec{\sigma}_h$ being the spin operators for the electron and hole, respectively. H_1 is the operator deduced by Bir and Pikus[13] and takes into account the effects of uniaxial stress. a, b, and d are the hydrostatic, tetragonal, and trigonal deformation potentials, respectively. e_{ij} are the components of the strain tensor and c.p. denotes cyclic permutation with respect to x, y, and z. The first term of H_1 describes the difference of the hydrostatic shifts of the conduction and valence bands; the second and third terms lead to stress-induced splittings of the Γ_8 valence bands.

The matrix elements of H are calculated on the basis of the eight $1S$ excitons in the jj-coupling scheme. From the 8×8 matrix of H the exciton energies, eigenvectors, and oscillator strengths for a given value and direction of the stress are derived. The eigenenergies $E_{i,n}$ and oscillator strengths $F_{i,n}$ determine the components ε_{ii} of the dielectric tensor which has only diagonal components in the system of the principal axes:

$$\varepsilon_{ii}(E) = \varepsilon_b + \sum_n \frac{F_{i,n}}{E_{i,n}^2 - E^2}. \quad (5)$$

ε_b is the background dielectric constant. The sum in Eq.

(5) is extended over all eigenstates with singlet admixture. For stress $\tau = 0$ Pa only the dipole-allowed orthoexcitons have oscillator strength. For finite stress, however, the paraexcitons also attain oscillator strength originating from a stress-induced mixing with the orthoexcitons.

Uniaxial stress causes strain in the crystal and lowers its symmetry. For stress in [001], [111], and [11$\bar{2}$] directions the corresponding point groups are D_{2d}, C_{3v}, or C_s, respectively. The resonances on the polariton dispersion curves can be calculated by solving the macroscopic Maxwell equations as described in Ref. 14. For stress directions [001] and [111] the dielectric tensor consists of two different diagonal elements and the crystal becomes uniaxial, whereas for [11$\bar{2}$] direction all components are different and the crystal becomes biaxial:

$$\hat{\varepsilon} = \begin{pmatrix} \varepsilon_{11} & 0 & 0 \\ 0 & \varepsilon_{22} & 0 \\ 0 & 0 & \varepsilon_{33} \end{pmatrix}. \tag{6}$$

$\varepsilon_{11} \neq \varepsilon_{22} = \varepsilon_{33}$ for stress directions [001] and [111], and $\varepsilon_{11} \neq \varepsilon_{22} \neq \varepsilon_{33} \neq \varepsilon_{11}$ for stress direction [11$\bar{2}$]. The principal axes of the dielectric tensor are shown in Fig. 2. In configurations **A**, **B**, and **C** the total k vector is parallel to a principal axis of the dielectric tensor and Maxwell's equations lead to the dispersion formula of pure transverse and longitudinal waves:

$$\varepsilon_{11} = \frac{k^2c^2}{\omega^2}, \quad \varepsilon_{33} = \frac{k^2c^2}{\omega^2} \text{ for transverse states,} \tag{7}$$

$$\varepsilon_{22} = 0 \quad \text{for longitudinal states.} \tag{8}$$

For configuration **D** the total k vector is not parallel to a principal axis of the dielectric tensor and waves with a polarization perpendicular to the $\vec{e}_2$ axis are longitudinal-transverse mixed, whereas waves with a polarization parallel to the $\vec{e}_2$ axis are pure transverse states. In this case Maxwell's equations lead to

$$\varepsilon_{22} = \frac{c^2k^2}{\omega^2} \tag{9}$$

for pure transverse states, whereas for longitudinal-transverse mixed states we get

$$\frac{\varepsilon_{11}\varepsilon_{33}}{\varepsilon_{11}\sin^2\varphi + \varepsilon_{33}\cos^2\varphi} = \frac{c^2k^2}{\omega^2}. \tag{10}$$

φ is the angle between the total k vector and $\vec{e}_3$. The angle can be calculated by diagonalization of the Hamilton matrix for stress direction [11$\bar{2}$]. In first order of approximation it is independent of the stress and exchange energy. The angle φ is a function of the elastic constants s_{11}, s_{22}, s_{44} and the tetragonal and trigonal deformation potentials b and d. φ can be calculated from the following equations:

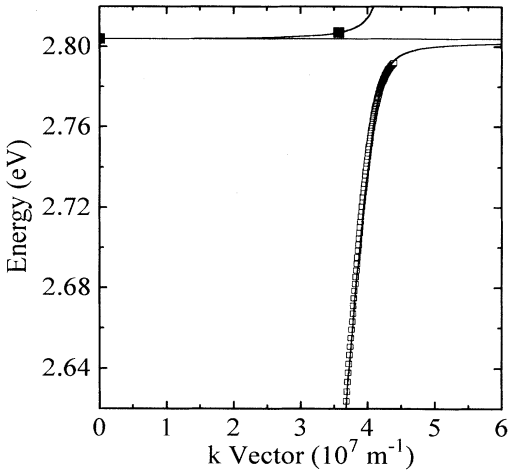

FIG. 3. Polariton dispersion curves of ZnSe at zero stress (solid lines). Solid squares represent resonances measured by two-photon excitation spectroscopy, open squares refer to measurements of nonresonant second-harmonic generation.

$$\tan\varphi = \frac{2}{Z + \sqrt{Z^2 + 4}}, \qquad \text{with} \quad Z = \frac{1}{\sqrt{2}} \frac{2(s_{11} - s_{12})b + 5s_{44}d}{2(s_{11} - s_{12})b - s_{44}d}. \tag{11}$$

We get $\varphi = 2°$ for ZnSe.

IV. RESULTS AND DISCUSSION

In Fig. 3 we present the dispersion curve of ZnSe without an external perturbation. We have used a Sellmeyer formula with two oscillators (orthoexciton and a phenomenological background oscillator which represents resonances at higher energies):

$$\frac{\hbar^2c^2k^2}{E^2} = \varepsilon = \varepsilon_b + \frac{F_1}{E_{T1}^2 - E^2} + \frac{F_2}{E_{T2}^2 - E^2}. \tag{12}$$

The nonlinear resonances on the upper polariton branch and the nonresonant second-harmonic generation on the lower polariton branch are very well reproduced by the polariton dispersion calculated from Eq. (12). The parameters of the polariton dispersion are listed in Table I.

TABLE I. Parameters of the polariton dispersion.

Oscillator	Parameter		
1S exciton	E_{T1}	(eV)	2.8026 ± 0.0001
	E_{L1}	(eV)	2.8038 ± 0.0001
	F_1	(eV^2)	0.0582 ± 0.0004
Background oscillator	E_{T2}	(eV)	3.148 ± 0.007
	E_{L2}	(eV)	3.33 ± 0.01
	F_2	(eV^2)	6.45 ± 0.04
Dielectric constant	ε_b		5.50 ± 0.02

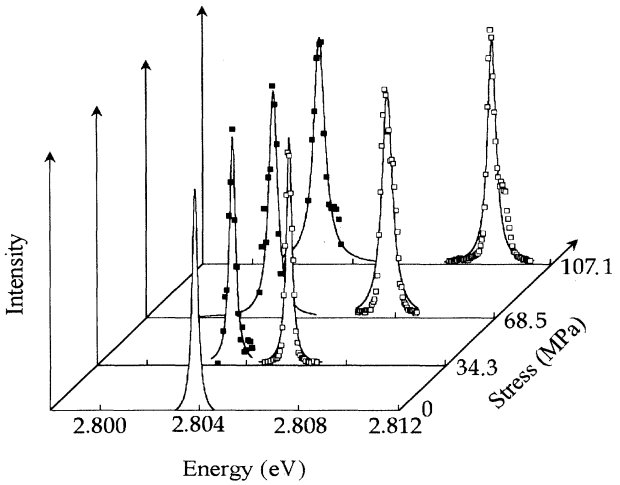

FIG. 4. Stress-induced splitting of the resonance at $\vec{k} = \vec{0}$ as measured in configuration **A** (Fig. 2). The two components can be excited separately by use of proper polarizations of the laser beam. Solid and open squares denote polarization parallel [001] and [110], respectively.

The longitudinal-transverse splitting of the orthoexciton (1.2 meV) is chosen according to Mayer *et al.*[15]

Mang, Reimann, and Rübenacke[16] determined for the longitudinal exciton energy $E_{L1} = (2.803\,55 \pm 0.000\,05)$ eV. This value is 0.25 meV lower than our value. The discrepancy is probably caused by the fact that Mang, Reimann, and Rübenacke[16] used polycrystalline samples whereas we used single crystals.

As an example we show in Fig. 4 the stress-induced splitting for the resonance at $\vec{k} = \vec{0}$ of configuration **A**. The components can be excited separately by use of different polarizations of the laser beam. The two-photon selection rules are given in detail in Ref. 17.

For the analysis of experimental results under uniaxial stress we use the elastic constants[18] $s_{11} = 2.018 \times 10^{-11}\,\mathrm{Pa}^{-1}$, $s_{12} = -0.752 \times 10^{-11}\,\mathrm{Pa}^{-1}$, and $s_{44} = 2.415 \times 10^{-11}\,\mathrm{Pa}^{-1}$. The parameter Δ_{ex}=0.33 meV of the Hamiltonian H_{ex} (Eq. 3) is determined by the energy of the paraexciton at zero stress and results from an extrapolation of the experimental data to zero stress.

According to Eq. (4), the second term vanishes for configuration **A** and the third for configuration **B**. Thus, for these configurations there remain only *two* adjustable parameters: the hydrostatic and tetragonal deformation potentials for [001] stress direction and the hydrostatic and trigonal deformation potentials for the stress axis parallel to [111]. The values for a, b, and d resulting from a least-squares fit are listed in Table II. Solid curves in the left-hand part of Fig. 5 show the result of this fit. Good agreement with our experimental data is achieved.

From the analysis of the experimental data of configurations **A** and **B** the deformation potentials are completely determined. Accordingly, one can calculate the theoretical values of the resonances for configurations **C** and **D** using these deformation potentials. Solid curves in the right-hand part of Fig. 5 show the result of this calculation. There is good agreement with the measured values which thus confirms very well our results for the deformation potentials. For comparison we present the results of other authors in Table II. The hydrostatic deformation potential a is determined by measurements of Mang, Reimann, and Rübenacke,[16] who studied the shift of the longitudinal $1S$ exciton under hydrostatic pressure up to 8 GPa. There is good agreement with our data. The hydrostatic deformation potential measured by Mang, Reimann, and Rübenacke[16] is of higher accuracy because there is only *one* adjustable parameter for their data analysis and the diamond anvil cell allows a much higher pressure. Euwema and Langer[19] derived the deformation potentials from reflectivity measurements

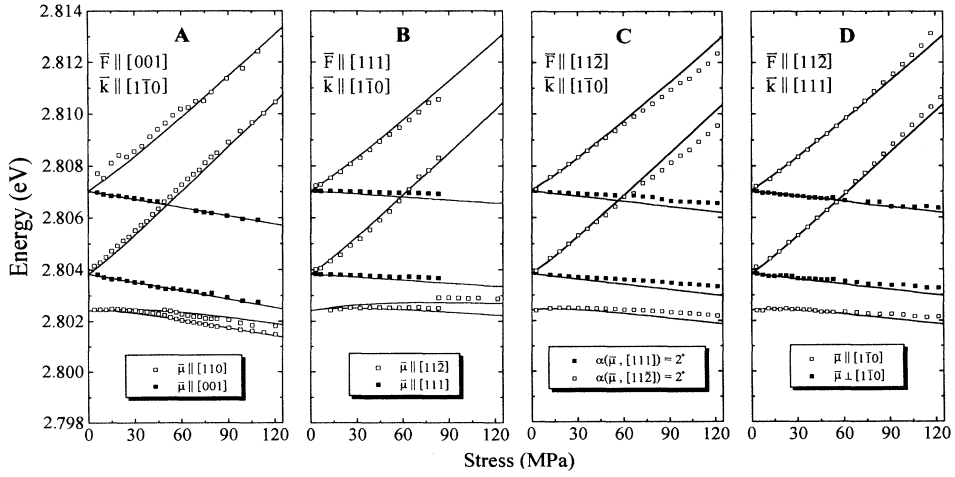

FIG. 5. Stress-dependent shift and splitting of resonances with different polarizations $\vec{\mu}$ for configurations **A**–**D**. The solid lines in configuration **A** and **B** are the result of a least-squares fit whereas the solid lines of configurations **C** and **D** are calculated with parameters derived from measurements in configurations **A** and **B**.

TABLE II. Deformation potentials of ZnSe. The values of Euwema and Langer are recalculated by the use of the elastic constants of Ref. 18. The different conventions for the definition of the deformation potentials in the Pikus-Bir Hamiltonian are taken into account.

Deformation potential	This work	Euwema and Langer[a]	Mang, Reimann and Rübenacke[b]
a (eV)	-4.7 ± 0.2	-5.9	-4.54 ± 0.02
b (eV)	3.72 ± 0.02	4.0	
d (eV)	7.36 ± 0.08	6.2	

[a]Reference 19; reflection under uniaxial stress at $T = 1.8$ K.
[b]Reference 16; two-photon absorption under hydrostatic pressure at $T = 6$ K.

under uniaxial stress. Compared with the results of this work there is a significant discrepancy. Since the analysis of reflection spectra requires the use of Kramers-Kronig relations and since the linewidths of resonances in reflection are about ten times larger than those of the resonances of the nonlinear measurements in this work, we are convinced that our deformation potentials are more reliable.

ACKNOWLEDGMENTS

The authors thank K. Reimann and St. Rübenacke for stimulating discussions. The financial support of this project by the Deutsche Forschungsgemeinschaft and the support of two of the authors (W.N. and J.W.) by the Graduiertenkolleg "Festkörperspektroskopie" are greatly appreciated.

[1] M. A. Haase, J. Qiu, J. M. DePuydt, and H. Cheng, Appl. Phys. Lett. **59**, 1272 (1991).
[2] H. Jeon, J. Ding, W. Patterson, A. V. Nurmikko, W. Xie, D. C. Grillo, M. Kobayashi, and R. L. Gunshor, Appl. Phys. Lett. **59**, 3619 (1991).
[3] S. Itoh, H. Okuyama, S. Matsumoto, N. N. Nakayama, T. Ohata, T. Miyajima, A. Ishibashi, and K. Akimoto, Electron. Lett. **29**, 766 (1993).
[4] N. Nakayama, S. Itoh, T. Ohata, K. Nakano, H. Okuyama, M. Ozawa, A. Ishibashi, M. Ikeda, and Y. Mori, Electron. Lett. **29**, 1488 (1993).
[5] A. Salokatve, H. Jeon, J. Ding, M. Hovinen, A. V. Nurmikko, D. C. Grillo, Li He, J. Han, Y. Fan, M. Ringle, R. L. Gunshor, G. C. Hua, and N. Otsuka, Electron. Lett. **29**, 2192 (1993).
[6] G. Landwehr and D. Hommel, Phys. Status Solidi B **187**, 269 (1995).
[7] D. Fröhlich, W. Nieswand, and St. Rübenacke, Phys. Rev. B **47**, 6736 (1993).
[8] D. Fröhlich and W. Nieswand, Philos. Mag. B **70**, 321 (1994).
[9] D. T. F. Marple, M. Aven, G. E. Hite, and B. Segall, Phys. Rev. **156**, 850 (1966).
[10] E. V. Markov and A. A. Davydov, Neorg. Mater. **11**, 1755 (1975).
[11] G. F. Koster, J. O. Dimmock, R. G. Wheeler, and H. Statz, *Properties of the Thirty-Two Point Groups* (M.I.T. Press, Cambridge, MA, 1963).
[12] K. Cho, Phys. Rev. B **14**, 4463 (1976).
[13] G. L. Bir and G. E. Pikus, *Symmetry and Strain-Induced Effects in Semiconductors* (Wiley, New York, 1974).
[14] M. Fiebig, D. Fröhlich, and Ch. Pahlke-Lerch, Phys. Status Solidi B **177**, 187 (1993).
[15] H. Mayer, U. Rössler, S. Permogorov, H. Stolz, H. Vogelsang, and W. von der Osten, J. Cryst. Growth **138**, 195 (1994).
[16] A. Mang, K. Reimann, and St. Rübenacke, in *Proceedings of the 22nd International Conference on the Physics of Semiconductors, Vancouver*, edited by D. J. Lockwood (World Scientific, Singapore, 1995), Vol. 1, p. 317.
[17] D. Fröhlich, F. Kubacki, M. Schlierkamp, H. Mayer, and U. Rössler, Phys. Status Solidi B **177**, 379 (1993).
[18] B. H. Lee, J. Appl. Phys. **41**, 2984 (1970).
[19] R. N. Euwema and D. W. Langer, Phys. Rev. B **2**, 4005 (1970).